

# Physics-Infused Reduced-Order Modeling for Analysis of Ablating Hypersonic Thermal Protection Systems

October 17, 2025

## Abstract

This work presents a physics-infused reduced-order modeling (PIROM) framework towards the design, analysis, and optimization of non-decomposing ablating hypersonic thermal protection systems (TPS).

## 1 Introduction

At hypersonic speeds, aerospace vehicles experience extreme aero-thermal environments that requires specialized thermal protection systems (TPS) to shield internal sub-structures, electronics, and possibly crew members from the intense aerodynamic heating. The TPS is often composed of ablating materials – a high-temperature capable fibrous material injected with a resin that fills the pore network and strengthens the composite [Amar2016](#). The TPS design promotes the exchange of mass through thermal and chemical reactions (i.e., pyrolysis), effectively mitigating heat transfer to the sub-structures.

As a result, accurate prediction for the ablating TPS response under extreme hypersonic heating becomes fundamental to ensuring survivability, performance, and safety of hypersonic vehicles. Not only is it necessary to assess the performance of the thermal management systems, but also the shape changes of the vehicle’s outer surface induced by the ablating material, and its impact on the aerodynamics, structural integrity, and controllability. Unfortunately, high-fidelity simulations of ablating TPS remains a formidable challenge both theoretically and computationally.

On the theoretical side, the thermo-chemical reactions, coupled with the irregular pore network structure, translate into simplifying assumptions to reduce non-linearities, and make the resulting equations more amenable for engineering application and design analysis [x](#). For instance, one of the most notable codes is the one-dimensional [CMA](#) code that was

developed by Aerotherm Corporation in the 1960s [Howard2015](#). Despite its practical use in...

Another example is the CHarring Ablator Response (CHAR) ablation code, which ignores elemental decompositions of the pyrolyzing gases, assumes the gases to be a mixture of perfect gases in thermal equilibrium, and assumes no reaction or condensation with the porous network [?].

theoretically:

computationally:

## 2 Modeling of Ablating Thermal Protection Systems

This section presents the problem of modeling ablation for a non-decomposing TPS as a parametrized system of coupled non-linear PDEs. The ablation physics is decomposed into heat conduction and mesh motion, which are governed by the energy and pseudo-elasticity PDEs, respectively. Predictions for the ablating TPS response computed based on two models: (1) a high-fidelity FOM based on discontinuous Galerkin FEM (DG-FEM), and (2) an RPM based on the LCM. The mathematical details for the governing equations, FOM, and RPM, are provided next.

### 2.1 Governing Equations

**Heat Conduction** Consider a generic domain  $\Omega \subset \mathbb{R}^d$ ,  $d = 2$  or  $3$ , illustrated in Fig. 1. Let  $\partial\Omega = \Gamma_q \cup \Gamma_T$  and  $\Gamma_q \cap \Gamma_T = \emptyset$ , where a Neumann  $q_b(x, t)$  boundary condition is prescribed on the  $\Gamma_q$  boundary, and a Dirichlet  $T_b(x, t)$  boundary condition is prescribed on the boundary  $\Gamma_T$ . The ablation is modeled as mesh motion, and occurs only on the heated boundary  $\Gamma_q$ . Ablating effects on the energy equation are handled using the Arbitrary Lagrangian-Eulerian (ALE) description. The ALE establishes that mesh displacements  $w(x, t) \in \mathbb{R}^d$  and velocities  $v(x, t) \in \mathbb{R}^d$  evolve independently of the physical material's displacements, which are set to zero [CITE](#).

The transient heat conduction is described by the energy equation,

$$\rho c_p \left( \frac{\partial T}{\partial t} - v(x, t) \cdot \nabla T \right) - \nabla \cdot (\mathbf{k} \nabla T) = \mathcal{Q}(x, t), \quad x \in \Omega \quad (1a)$$

$$-\mathbf{k} \nabla T \cdot \mathbf{n} = q_b(x, t), \quad x \in \Gamma_q \quad (1b)$$

$$T(x, t) = T_b(x, t), \quad x \in \Gamma_T \quad (1c)$$

$$T(x, 0) = T_0(x), \quad x \in \Omega \quad (1d)$$

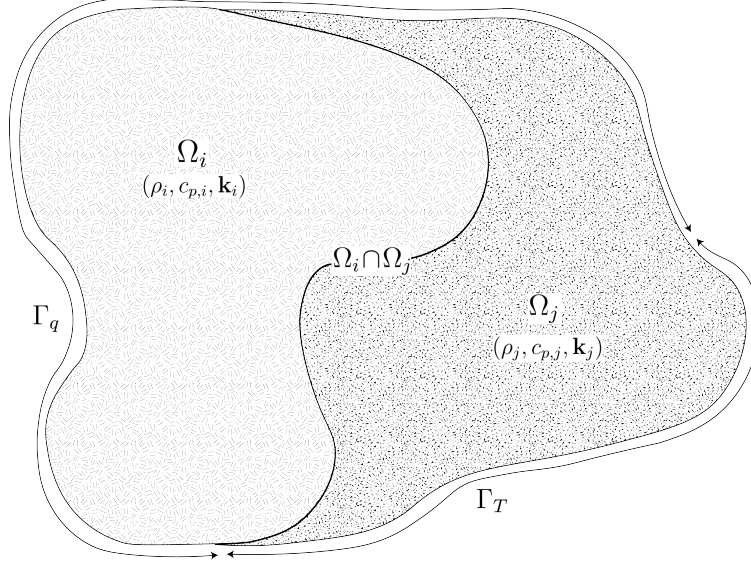


Figure 1: General domain  $\Omega$  with prescribed Neumann and Dirichlet boundary conditions on  $\Gamma_q$  and  $\Gamma_T$ . Mesh displacement  $w(x, t)$  occurs on the  $\Gamma_q$  boundary.

54 where the density  $\rho$  is constant, while the heat capacity  $c_p$  and thermal conductivity  $\mathbf{k} \in$   
55  $\mathbb{R}^{d \times d}$ , are temperature dependent. In the order they appear, the terms in eq. (1a) include, the  
56 unsteady energy storage, heat conduction, temperature advection due to mesh motion, and  
57 source terms due to boundary conditions. The boundary conditions for the energy equation  
58 includes Neumann eq. (1b) on  $\Gamma_1$  and Dirichlet eq. (1c) on  $\Gamma_T$ .

59 **Mesh Motion** The mesh motion is described by the pseudo-elasticity equation,

$$\nabla \cdot \sigma(w) = 0 \quad (2a)$$

$$w(x, t) = w_q(x, t), \quad x \in \Gamma_q \quad (2b)$$

$$w(x, t) = 0, \quad x \notin \Gamma_q \quad (2c)$$

$$w(x, 0) = \mathbf{0} \quad (2d)$$

60 where the stress tensor  $\sigma$  is related to the strain tensor  $\epsilon(w)$  through Hooke's law,

$$\sigma(w) = \mathbb{D} : \epsilon(w)$$

61 where  $\mathbb{D}$  is the constitutive operator, “:” is the double contraction of tensors, and  $\epsilon$  is the  
62 symmetric strain tensor given by,

$$\epsilon(\mathbf{w}) = \frac{1}{2} (\nabla \mathbf{w} + \nabla \mathbf{w}^T)$$

The “material” properties for the mesh are chosen to tailor the mesh deformation, and need not represent the actual material being modeled [Amar2016](#).

For the pseudo-elasticity equations, the surface velocity due to the ablating material is a function of the surface temperature  $T_q(x, t)$  for  $x \in \Gamma_q$  on the heated boundary. For the  $i$ -th material component, the surface velocity is imposed based on the following relation,

$$\hat{\mathbf{n}} \cdot \mathbf{v}(x, t) = f(T_q(x, t)), \quad x \in \Gamma_q \quad (3)$$

where  $\hat{\mathbf{n}}$  is the unit normal vector on the heated boundary  $\Gamma_q$ , and  $f$  is a function obtained from tabulated data for the material, commonly referred to as a B’ table. The B’ table provides the recession velocity as a function of surface temperature, and is pre-computed based on high-fidelity simulations of the ablation process for a one-dimensional slab of the material, and is independent of the TPS geometry and boundary conditions. The surface displacements are then computed by integrating the surface velocities over time,

$$\mathbf{w}_q(x, t) = \int_0^t \mathbf{v}(x, \tau) d\tau = \int_0^t f(T_q(x, \tau)) d\tau \quad (4)$$

## 2.2 Full-Order Model: Finite-Element Method

To obtain the full-order numerical solution, the governing equation is spatially discretized using variational principles of Discontinuous Galerkin (DG) to result in a high-dimensional system of ordinary differential equations (ODEs). Note that the choice of DG approach here is mainly for theoretical convenience in the coarse-graining formulation, and is exclusively performed on the energy equation as the quantities of interest correspond to the ablating surface temperatures. In Sec. [x](#), the high-fidelity ablating TPS solution is performed using standard FEM for both the energy and elasticity equations, and the equivalence between DG and standard FEM is noted upon their convergence.

Consider a conforming mesh partition domain, where each element belongs to one and only one component. Denote the collection of all  $M$  elements as  $\{E_i\}_{i=1}^M$ . In an element  $E_i$ , its shared boundaries with another element  $E_j$ , Neumann BC, and Dirichlet BC are denoted as  $e_{ij}$ ,  $e_{iq}$ , and  $e_{iT}$ , respectively. Lastly,  $|e|$  denotes the length ( $n_d = 2$ ) or area ( $n_d = 3$ ) of a component boundary  $e$ .

For the  $i$ -th element, use a set of  $P$  trial functions, such as polynomials, to represent the temperature distribution,

$$T^{(i)}(x, t) = \sum_{l=1}^P \phi_l^{(i)}(x) u_l^{(i)} \equiv \boldsymbol{\phi}^{(i)}(x)^T \mathbf{u}^{(i)}(t), \quad i = 1, 2, \dots, M \quad (5)$$

By standard variational processes, e.g., [Cohen2018](#), the element-wise governing equation is denoted as,

$$\mathbf{A}^{(i)} \dot{\mathbf{u}}^{(i)} = (\mathbf{B}^{(i)} + \mathbf{C}^{(i)}) \mathbf{u}^{(i)} + \sum_{j \in \mathcal{N}_i \cup \{T_b\}} (\mathbf{B}_{ij}^{(i)} \mathbf{u}^{(i)} + \mathbf{B}_{ij}^{(j)} \mathbf{u}^{(j)}) + \mathbf{f}^{(i)}(t), \quad \text{for } i = 1, 2, \dots, M \quad (6)$$

which is collected as the following ODE for the all the elements in the mesh,

$$\mathbf{A}(\mathbf{u}) \dot{\mathbf{u}} = [\mathbf{B}(\mathbf{u}) + \mathbf{C}(\mathbf{u})] \mathbf{u} + \mathbf{f}(t) \quad (7)$$

where  $\mathbf{u} = [\mathbf{u}^{(1)}, \mathbf{u}^{(2)}, \dots, \mathbf{u}^{(M)}]^T \in \mathbb{R}^{MP}$  includes all the DG variables,  $\mathbf{f} \in \mathbb{R}^{MP}$  is the external forcing, and the system matrices  $\mathbf{A}$ ,  $\mathbf{B}$ , and  $\mathbf{C}$  are the matrices due to heat capacity, heat conduction, and temperature advection due to mesh motion, respectively. A detailed derivation of eqs. (6) and (7) and their matrices is provided in Appendix [?].

## 2.3 Reduced-Physics Model

The RPM for predicting the response of the ablating TPS consists of two components: (1) the LCM, and (2) tabulated data for ablating velocity as a function of surface temperature. The LCM is described as a first-order system of ODEs for predicting the average temperatures inside the ablating TPS, and provides a low-fidelity under-estimation for the ablating surface temperature. The temperature prediction from LCM is used in a B' table to determine the surface recession velocity, from which the displacements are obtained through integration.

### 2.3.1 Lumped Capacitance Model

The main results regarding the LCM are provided in this section; details of the implementation for the TPS in Fig. 2 are provided in Appendix A. The LCM is a classical physics-based low-order model for predicting the temporal variation of average temperature in multiple interconnected components [INCROPERA](#). The LCM is derived at the component level from a point of view of energy conservation, and leads to the following system of ODEs for the average temperatures on the components,

$$\bar{\mathbf{A}} \dot{\bar{\mathbf{u}}} = \bar{\mathbf{B}}(\bar{\mathbf{u}}) \bar{\mathbf{u}} + \bar{\mathbf{f}}(t) \quad (8)$$

111 where,

$$\bar{\mathbf{u}} = [\bar{u}^{(1)}, \bar{u}^{(2)}, \dots, \bar{u}^{(N)}]^T \in \mathbb{R}^N \quad (9a)$$

$$\bar{\mathbf{f}} = [\bar{f}^{(1)}, \bar{f}^{(2)}, \dots, \bar{f}^{(N)}]^T \in \mathbb{R}^N \quad (9b)$$

112 includes the average temperatures  $\bar{\mathbf{u}}$  and forcing inputs  $\bar{\mathbf{f}}$  for the  $N$  components. For  $i, j =$   
 113  $1, 2, \dots, N$  the  $(i, j)$ -th elements of the  $\bar{\mathbf{A}} \in \mathbb{R}^{N \times N}$ ,  $\bar{\mathbf{B}} \in \mathbb{R}^{N \times N}$ , and  $\bar{\mathbf{f}} \in \mathbb{R}^N$  matrices are  
 114 given by,

$$\bar{A}^{(i)} = \begin{cases} \int_{\Omega^{(i)}} \rho c_p d\Omega^{(i)}, & i = j \\ 0, & i \neq j \end{cases}, \quad \bar{B}_{ij} = \begin{cases} \sum_{j \in \mathcal{N}_i \cup \{T_b\}} \bar{B}_{ij}^{(i)}, & i = j \\ \bar{B}_{ij}^{(j)}, & i \neq j \end{cases}, \quad (10a)$$

$$\mathbf{f}^{(i)} = \begin{cases} |e_{iq}| \bar{q}^{(i)} + \frac{|e_{iT}|}{R_i} \bar{T}^{(i)}, & i = j \\ 0, & i \neq j \end{cases} \quad (10b)$$

115 where,

$$\bar{q}^{(i)} = \frac{1}{|e_{iq}|} \int_{e_{iq}} q_b de_{iq}, \quad \bar{T}^{(i)} = \frac{1}{|e_{iT}|} \int_{e_{iT}} T_b de_{iT}, \quad \bar{B}_{ij}^{(i)} = -\frac{|e_{ij}|}{R_{ij}}, \quad \bar{B}_{ij}^{(j)} = \frac{|e_{ij}|}{R_{ij}} \quad (11)$$

### 116 2.3.2 Surface Recession Velocity and Displacements

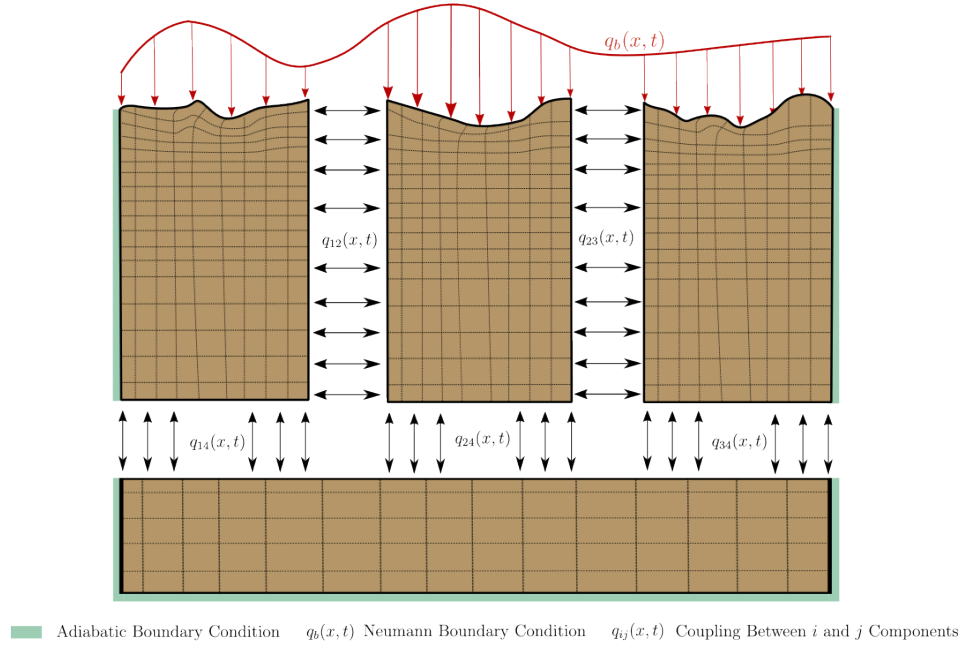
117 The surface velocity on the heated boundary  $\Gamma_q$  is computed based on the temperature  
 118 predicted by the LCM using eq. (3). Thus, based on the  $i$ -th average temperature  $\bar{u}^{(i)}$ , the  
 119 wall-normal surface velocity is computed as,

$$\hat{\mathbf{n}} \cdot \mathbf{v}^{(i)}(x, t) = f(\bar{u}^{(i)}(t)) \quad (12)$$

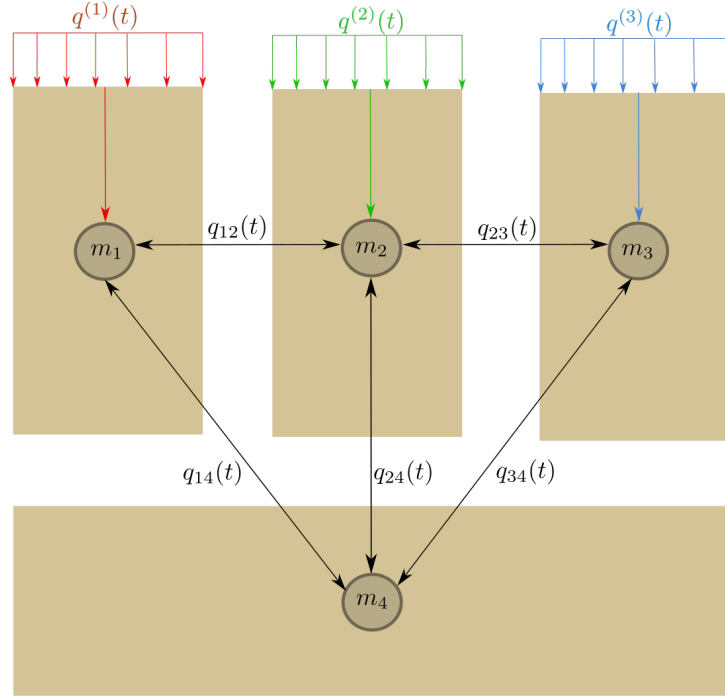
120 Due

## 121 2.4 Summary of Modeling Approaches

122 The FOM (i.e., DG-FEM) and RPM (i.e., LCM) are two different but mathematically con-  
 123 nected solution strategies. Specifically, the LCM in eq. (8) not only resembles the functional  
 124 form of the DG model in eq. (7), but can be viewed as a special case of the latter, where the  
 125 mesh partition is extremely coarse, and the trial and test functions are piece-wise constants.  
 126 For example, consider the case where each component  $\Omega^{(i)}$  is treated as one single element,  
 127 and each element employs one constant basis function  $\phi^{(i)} = 1$ . The element-wise DG model



(a) TPS Decomposition



(b) Lumped Mass Representation

Figure 2: Partition of the TPS into three ablating and one non-ablating components with the corresponding lumped-mass representation.

in eq. (6) simplifies into a scalar ODE that ignores advection effects due to mesh motion,

$$\mathbf{A}^{(i)} = \bar{\mathbf{A}}^{(i)}, \quad \mathbf{C}^{(i)} = 0, \quad \mathbf{B}_{ij}^{(i)} = -\sigma|e_{ij}|, \quad \mathbf{B}_{ij}^{(j)} = \sigma|e_{ij}|, \quad \mathbf{f}^{(i)} = |e_{iq}|\bar{q}^{(i)} + \sigma|e_{iT}|\bar{T}^{(i)} \quad (13)$$

Clearly, the LCM is a coarse zeroth-order DG model with the inverse of thermal resistance chosen as the element-wise penalty factors. Or conversely, the DG model is a refined version of LCM via *hp*-adaptation.

The FOM and RPM represent two extremes in the modeling fidelity and computational cost spectrum. On one hand, the FOM is the most accurate but computationally expensive to evaluate due to the fine mesh discretizations for both the temperature and displacement fields, leading to possibly millions of state variables. On the other hand, the RPM considers only the average temperature of the material as the state variable, considerably reducing the computational cost, but sacrificing local temperature information and thus neglecting higher-order effects due to mesh motion. Thus, neither the FOM nor the RPM is a universal approach for real-world analysis, design, and optimization tasks for ablating TPS, where thousands of high-fidelity model evaluations may be necessary. This issue motivates the development of the PIROM, which can achieve the fidelity of FOM at a computational cost close to the RPM, while maintaining the generalizability to model parameters.

### 3 Physics-Infused Reduced-Order Modeling

The formulation of PIROM for ablating TPS starts by connecting the FOM, i.e., DG-FEM, and the RPM, i.e., the LCM, via a coarse-graining procedure. This procedure pinpoints the missing dynamics in the LCM when compared to DG-FEM. Subsequently, the Mori-Zwanzig (MZ) formalism is employed to determine the model form for the missing dynamics in PIROM. Lastly, the data-driven identification of the missing dynamics in PIROM is presented.

#### 3.1 Deriving the Reduced-Physics Model via Coarse-Graining

The LCM is derived from a full-order DG on a fine mesh via coarse graining. This process constraints the trial function space of a full-order DG model to a subset of piece-wise constants, so that the variables  $\mathbf{u}$ , matrices  $\mathbf{A}$ ,  $\mathbf{B}$ , and  $\mathbf{C}$ , and forcing vector  $\mathbf{f}$  are all approximated using a single state associated to the average temperature. The details of the projection are described next.



### 3.1.1 Coarse-Graining of States

Consider a DG model as in eq. (7) for  $M$  elements and an LCM as in eq. (8) for  $N$  components; clearly  $M \gg N$ . Let  $\mathcal{V}_j = \{i | E_i \in \Omega_j\}$  be the indices of the elements belonging to the  $j$ -th component, so  $E_i \in \Omega_j$  for all  $i \in \mathcal{V}_j$ . The number of elements in the  $j$ -th component is  $|\mathcal{V}_j|$ . The average temperature on  $\Omega_j$  is,

$$\bar{u}_j = \frac{1}{|\Omega_j|} \sum_{i \in \mathcal{V}_j} \int_{E(i)} \phi^{(i)}(x)^T \mathbf{u}^{(i)} d\Omega = \frac{1}{|\Omega_j|} \sum_{i \in \mathcal{V}_j} |E_i| \boldsymbol{\varphi}_i^{j\top} \mathbf{u}^{(i)}, \quad j = 1, 2, \dots, N \quad (14)$$

where  $|\Omega_j|$  and  $|E_i|$  denote the area ( $d = 2$ ) or volume ( $d = 3$ ) of component  $j$  and element  $i$ , respectively. The orthogonal basis functions are defined as  $\boldsymbol{\varphi}_i^{j\top} = [1, 0, \dots, 0]^\top \in \mathbb{R}^P$ .

Conversely, given the average temperatures of the  $N$  components,  $\bar{\mathbf{u}}$ , the states of an arbitrary element  $E_i$  is written as,

$$\mathbf{u}^{(i)} = \sum_{k=1}^N \boldsymbol{\varphi}_i^k \bar{u}_k + \delta \mathbf{u}^{(i)}, \quad i = 1, 2, \dots, M \quad (15)$$

where  $\boldsymbol{\varphi}_i^k = 0$  if  $i \notin \mathcal{V}_k$ , and  $\delta \mathbf{u}^{(i)}$  represents the deviation from the average temperature and satisfies the orthogonality condition  $\boldsymbol{\varphi}_i^{k\top} \delta \mathbf{u}^{(i)} = 0$  for all  $k$ .

Equations eqs. (14) and (15) are combined and written in matrix form as,

$$\bar{\mathbf{u}} = \boldsymbol{\Phi}^+ \mathbf{u}, \quad \mathbf{u} = \boldsymbol{\Phi} \mathbf{u} + \delta \mathbf{u} \quad (16)$$

where  $\boldsymbol{\Phi} \in \mathbb{R}^{MP \times N}$  is a matrix of  $M \times N$  blocks, with the  $(i, j)$ -th block as  $\boldsymbol{\varphi}_i^j$ ,  $\boldsymbol{\Phi}^+ \in \mathbb{R}^{N \times MP}$  is the left inverse of  $\boldsymbol{\Phi}$ , with the  $(i, j)$ -th block as  $\boldsymbol{\varphi}_i^{j+} = \frac{|E_i|}{|\Omega_j|} \boldsymbol{\varphi}_i^{j\top}$ , and  $\delta \mathbf{u}$  is the collection of deviations. By their definitions,  $\boldsymbol{\Phi}^+ \boldsymbol{\Phi} = \mathbf{I}$  and  $\boldsymbol{\Phi}^+ \delta \mathbf{u} = \mathbf{0}$ .

### 3.1.2 Coarse-Graining of Dynamics

Next, consider a function of states in the form of  $\mathbf{M}(\mathbf{u}) \mathbf{g}(\mathbf{u})$ , where  $\mathbf{g} : \mathbb{R}^{MP} \rightarrow \mathbb{R}^{MP}$  is a vector-valued function, and  $\mathbf{M} : \mathbb{R}^{MP} \rightarrow \mathbb{R}^{p \times MP}$  is a matrix-valued function with an arbitrary dimension  $p$ . Define the projection matrix  $\mathbf{P} = \boldsymbol{\Phi} \boldsymbol{\Phi}^+$  and the projection operator  $\mathcal{P}$  as,

$$\begin{aligned} \mathcal{P}[\mathbf{M}(\mathbf{u}) \mathbf{g}(\mathbf{u})] &= \mathbf{M}(\mathbf{P} \mathbf{u}) \mathbf{g}(\mathbf{P} \mathbf{u}) \\ &= \mathbf{M}(\boldsymbol{\Phi} \bar{\mathbf{u}}) \mathbf{g}(\boldsymbol{\Phi} \bar{\mathbf{u}}) \end{aligned} \quad (17)$$

so that the resulting function depends only on the average temperatures  $\bar{\mathbf{u}}$ . Correspondingly, the residual operator  $\mathcal{Q} = \mathcal{I} - \mathcal{P}$ , and  $\mathcal{Q}[\mathbf{M}(\mathbf{u})\mathbf{g}(\mathbf{u})] = \mathbf{M}(\mathbf{u})\mathbf{g}(\mathbf{u}) - \mathbf{M}(\Phi\bar{\mathbf{u}})\mathbf{g}(\Phi\bar{\mathbf{u}})$ . When the function is not separable, the projection operator is simply defined as  $\mathcal{P}[\mathbf{g}(\mathbf{u})] = \mathbf{g}(\mathbf{P}\mathbf{u})$ .

Subsequently, the operators defined above are applied to coarse-grain the dynamics. First, write the DG-FEM in eq. (7) as,

$$\dot{\mathbf{u}} = \mathbf{A}(\mathbf{u})^{-1}\mathbf{B}(\mathbf{u})\mathbf{u} + \mathbf{A}(\mathbf{u})^{-1}\mathbf{C}(\mathbf{u})\mathbf{u} + \mathbf{A}(\mathbf{u})^{-1}\mathbf{f}(t) \quad (18)$$

and multiply both sides by  $\Phi^+$  to obtain,

$$\Phi^+\dot{\mathbf{u}} = \Phi^+(\Phi\dot{\bar{\mathbf{u}}} + \delta\dot{\mathbf{u}}) = \dot{\bar{\mathbf{u}}} = \Phi^+\mathbf{r}(\mathbf{u}, t) \quad (19)$$

Apply the projection operator  $\mathcal{P}$  and the residual operator  $\mathcal{Q}$  to the right-hand side to obtain,

$$\dot{\bar{\mathbf{u}}} = \mathcal{P}[\Phi^+\mathbf{r}(\mathbf{u}, t)] + \mathcal{Q}[\Phi^+\mathbf{r}(\mathbf{u}, t)] \equiv \mathbf{r}^{(1)}(\mathbf{u}, t) + \mathbf{r}^{(2)}(\mathbf{u}, t) \quad (20)$$

where  $\mathbf{r}^{(1)}(\mathbf{u}, t)$  is resolved dynamics that depends on  $\bar{\mathbf{u}}$  only, and  $\mathbf{r}^{(2)}(\mathbf{u}, t)$  is the un-resolved or residual dynamics. Detailed derivations and analysis of  $\mathbf{r}^{(1)}(\mathbf{u}, t)$  and  $\mathbf{r}^{(2)}(\mathbf{u}, t)$  can be found in the Appendix.

It follows from Ref. [x](#) that the resolved dynamics is exactly the LCM, where the advection term reduces to zero, i.e.,  $\bar{\mathbf{C}}(\bar{\mathbf{u}}) = \mathbf{0}$  as shown in the Appendix. Using the notation from eq. (8), it follows that,

$$\begin{aligned} \mathbf{r}^{(1)}(\mathbf{u}, t) &= \bar{\mathbf{A}}(\bar{\mathbf{u}})^{-1}\bar{\mathbf{B}}(\bar{\mathbf{u}})\bar{\mathbf{u}} + \bar{\mathbf{A}}(\bar{\mathbf{u}})^{-1}\bar{\mathbf{C}}(\bar{\mathbf{u}})\bar{\mathbf{u}} + \bar{\mathbf{A}}(\bar{\mathbf{u}})^{-1}\bar{\mathbf{f}}(\bar{\mathbf{u}}) \\ &= \bar{\mathbf{A}}(\bar{\mathbf{u}})^{-1}\bar{\mathbf{B}}(\bar{\mathbf{u}})\bar{\mathbf{u}} + \bar{\mathbf{A}}(\bar{\mathbf{u}})^{-1}\bar{\mathbf{f}}(t) \end{aligned} \quad (21)$$

where the following relations hold,

$$\bar{\mathbf{A}}(\bar{\mathbf{u}}) = \mathbf{W}(\Phi^+\mathbf{A}(\Phi\bar{\mathbf{u}})^{-1}\Phi)^{-1} \quad \bar{\mathbf{C}}(\bar{\mathbf{u}}) = \mathbf{0} \quad (22a)$$

$$\bar{\mathbf{B}}(\bar{\mathbf{u}}) = \mathbf{W}\Phi^+\mathbf{B}(\Phi\bar{\mathbf{u}})\Phi \quad \bar{\mathbf{f}}(t) = \mathbf{W}\Phi^+\mathbf{f} \quad (22b)$$

where  $\mathbf{W} \in \mathbb{R}^{N \times N}$  is a diagonal matrix with the  $i$ -th element as  $[\mathbf{W}]_{ii} = |\mathcal{V}_k|$  if  $i \in \mathcal{V}_k$ . As shown in the Appendix, the examination of the second residual term  $\mathbf{r}^{(2)}(\mathbf{u}, t)$  in eq. (20) reveals the physical sources of missing dynamics in the LCM: the approximation of non-uniform temperature within each component as a constant, and the elimination of the advection term due to coarse-graining.

In sum, the above results not only show that the LCM is a result of coarse-graining of

the full-order DG-FEM, but also reveal the discrepancies between the LCM and the DG-FEM. In the subsequent section, the discrepancies will be corrected to produce the proposed PIROM.

### 3.2 Formulation of Reduced-Order Model

The Mori-Zwanzig (MZ) formalism is an operator-projection technique used to derive ROMs for high-dimensional dynamical systems, especially in statistical mechanics and fluid dynamics [Parish,Duraisamy](#). It provides an exact reformulation of the full-order dynamics in terms of a subset of resolved variables. The proposed ROM is subsequently developed based on such reformulation. Equation eq. (20) shows that the DG-FEM dynamics can be decomposed into the resolved dynamics  $\mathbf{r}^{(1)}(\mathbf{u}, t)$  and the orthogonal dynamics  $\mathbf{r}^{(2)}(\mathbf{u}, t)$ , in the sense of  $\mathcal{P}\mathbf{r}^{(2)} = 0$ . In this case, the MZ formalism can be invoked to express the dynamics  $\bar{\mathbf{u}}$  in terms of  $\bar{\mathbf{u}}$  alone as the projected Generalized Langevin Equation (GLE) [Parish,Duraisamy](#),

$$\dot{\bar{\mathbf{u}}}(t) = \mathbf{r}^{(1)}(\bar{\mathbf{u}}, t) + \int_0^t \tilde{\boldsymbol{\kappa}}(t, s, \bar{\mathbf{u}}) ds \quad (23)$$

where the first term is Markovian, and the integral term is referred to as the memory. The integral term is non-Markovian, accounting for impact of past resolved states on the current states through their interactions with the un-resolved states.

Next, to further inform the subsequent derivation of the ROM, the kernel  $\tilde{\boldsymbol{\kappa}}$  is examined via a leading-order expansion, based on prior work [x](#); this can be viewed as an analog of zeroth-order holding in linear system theory with a sufficiently small time step. In this case, the memory kernel is approximated as,

$$\tilde{\boldsymbol{\kappa}}(t, s, \bar{\mathbf{u}}) \approx \mathbf{r}^{(1)}(\bar{\mathbf{u}}, t) \cdot \nabla_{\bar{\mathbf{u}}} \mathbf{r}^{(2)}(\Phi \bar{\mathbf{u}}, t) \quad (24)$$

Note that the terms in  $\mathbf{r}^{(1)}$  have a common factor  $\bar{\mathbf{A}}^{-1}$ ; this motivates the following heuristic modification of the model form in eq. (23),

$$\dot{\bar{\mathbf{u}}} = \mathbf{r}^{(1)}(\bar{\mathbf{u}}, t) + \bar{\mathbf{A}}^{-1}(\bar{\mathbf{u}}) \int_0^t \boldsymbol{\kappa}(t, s, \bar{\mathbf{u}}) ds \quad (25a)$$

$$\bar{\mathbf{A}}(\bar{\mathbf{u}}) \dot{\bar{\mathbf{u}}} = \bar{\mathbf{B}}(\bar{\mathbf{u}}) \bar{\mathbf{u}} + \bar{\mathbf{f}}(t) + \int_0^t \boldsymbol{\kappa}(t, s, \bar{\mathbf{u}}) ds \quad (25b)$$

where the original kernel  $\tilde{\boldsymbol{\kappa}}$  is effectively normalized by  $\bar{\mathbf{A}}^{-1}$ . Intuitively, such choice of kernel reduces its dependency on the averaged material properties, and simplifies the subsequent design of model form.

Subsequently, the hidden states are introduced to “Markovianize” the system eq. (23). In this manner, eq. (25b) is converted into a pure state-space model, with the functional form of the LCM retained; since LCM is a physics-based model, then it encodes the physical information and retains explicit parametric dependence of the problem. Consider the representation of the kernel as a finite sum of simpler functions, e.g., exponentials,

$$\kappa(t, s, \bar{\mathbf{u}}) = \sum_{j=1}^m \mathcal{K}_j(t, s, \bar{\mathbf{u}}) [\mathbf{p}_j + \mathbf{d}_j(\bar{\mathbf{u}})] \phi_j(s, \bar{\mathbf{u}}) \quad (26)$$

where,

$$\mathcal{K}_j(t, s, \bar{\mathbf{u}}) = e^{-\int_s^t (\lambda_j + e_j(\bar{\mathbf{u}})) d\tau}, \quad \phi_j(s, \bar{\mathbf{u}}) = \mathbf{q}_j^\top \bar{\mathbf{u}}(s) + \mathbf{g}_j(\bar{\mathbf{u}})^\top \bar{\mathbf{u}}(s) + \mathbf{r}_j^\top \bar{\mathbf{f}}(s) \quad (27)$$

with suitable coefficients  $\mathbf{p}_j, \mathbf{d}_j, \mathbf{q}_j, \mathbf{g}_j, \mathbf{r}_j \in \mathbb{R}^N$  and decay rates  $\lambda_j, e_j(\bar{\mathbf{u}}) > 0$ , that need to be identified from data.

Define the hidden states as,

$$\beta_j(t) = \int_0^t \mathcal{K}_j(s, \bar{\mathbf{u}}) \phi_j(s, \bar{\mathbf{u}}) ds \quad (28)$$

then through its differentiation with respect to time,

$$\dot{\beta}_j(t) = -[\lambda_j + e_j(\bar{\mathbf{u}})] \beta_j(t) + \mathbf{q}_j^\top \bar{\mathbf{u}}(t) + \mathbf{g}_j(\bar{\mathbf{u}})^\top \bar{\mathbf{u}}(t) + \mathbf{r}_j^\top \bar{\mathbf{f}}(t) \quad (29)$$

and the memory term becomes,

$$\int_0^t \kappa(t, s, \bar{\mathbf{u}}) ds = \sum_{j=1}^m [\mathbf{p}_j + \mathbf{d}_j(\bar{\mathbf{u}})] \beta_j(t) \quad (30)$$

Then, eq. (25b) is recast as the extended Markovian system,

$$\bar{\mathbf{A}}(\bar{\mathbf{u}}) \dot{\bar{\mathbf{u}}} = \bar{\mathbf{B}}(\bar{\mathbf{u}}) \bar{\mathbf{u}} + [\mathbf{P} + \mathbf{D}(\bar{\mathbf{u}})] \boldsymbol{\beta} + \bar{\mathbf{f}}(t) \quad (31a)$$

$$\dot{\boldsymbol{\beta}} = [-\boldsymbol{\Lambda} + \mathbf{E}(\bar{\mathbf{u}})] \boldsymbol{\beta} + [\mathbf{Q} + \mathbf{G}(\bar{\mathbf{u}})] \bar{\mathbf{u}} + \mathbf{R} \bar{\mathbf{f}}(t) \quad (31b)$$

where,

$$\mathbf{\Lambda} = \text{diag}(\lambda_1, \lambda_2, \dots, \lambda_m) \in \mathbb{R}^{N \times m}, \quad \mathbf{P} = [\mathbf{p}_1, \mathbf{p}_2, \dots, \mathbf{p}_m] \in \mathbb{R}^{N \times m} \quad (32a)$$

$$\mathbf{D}(\bar{\mathbf{u}}) = [\mathbf{d}_1(\bar{\mathbf{u}}), \mathbf{d}_2(\bar{\mathbf{u}}), \dots, \mathbf{d}_m(\bar{\mathbf{u}})] \in \mathbb{R}^{N \times m}, \quad \mathbf{Q} = [\mathbf{q}_1, \mathbf{q}_2, \dots, \mathbf{q}_m] \in \mathbb{R}^{N \times m} \quad (32b)$$

$$\mathbf{G}(\bar{\mathbf{u}}) = [\mathbf{g}_1(\bar{\mathbf{u}}), \mathbf{g}_2(\bar{\mathbf{u}}), \dots, \mathbf{g}_m(\bar{\mathbf{u}})] \in \mathbb{R}^{N \times m}, \quad \mathbf{R} = [\mathbf{r}_1, \mathbf{r}_2, \dots, \mathbf{r}_m] \in \mathbb{R}^{N \times m} \quad (32c)$$

$$\mathbf{E}(\bar{\mathbf{u}}) = \text{diag}(e_1(\bar{\mathbf{u}}), e_2(\bar{\mathbf{u}}), \dots, e_m(\bar{\mathbf{u}})) \in \mathbb{R}^{m \times m} \quad (32d)$$

Since the hidden states  $\boldsymbol{\beta}$  serve as the memory, their initial conditions are set to zero, i.e.,  $\boldsymbol{\beta}(t_0) = \mathbf{0}$ , no memory at the beginning. The physics-infused model in eq. (31) retains the structure of the LCM, while the hidden states account for missing physics through corrections to the stiffness and advection matrices, as well as the forcing term.

Lastly, denote the collection of resolved and hidden states as  $\mathbf{y} = [\bar{\mathbf{u}}, \boldsymbol{\beta}]^T \in \mathbb{R}^{n_y}$  with  $n_y = N + m$ , then the proposed PIROM is summarized as,

$$\tilde{\mathbf{A}}\dot{\mathbf{y}} = [\tilde{\mathbf{B}} + \tilde{\mathbf{C}}] \mathbf{y} + \mathbf{H}\bar{\mathbf{f}}(t) \quad (33a)$$

$$\mathbf{z} = \mathbf{M}\mathbf{y} \quad (33b)$$

where,

$$\tilde{\mathbf{A}} = \begin{bmatrix} \bar{\mathbf{A}}(\bar{\mathbf{u}}) & \mathbf{O} \\ \mathbf{O} & \mathbf{I} \end{bmatrix} \in \mathbb{R}^{n_y \times n_y}, \quad \tilde{\mathbf{B}} = \begin{bmatrix} \bar{\mathbf{B}}(\bar{\mathbf{u}}) & \mathbf{P} \\ \mathbf{Q} & -\mathbf{\Lambda} \end{bmatrix} \in \mathbb{R}^{n_y \times n_y}, \quad \tilde{\mathbf{C}} = \begin{bmatrix} \mathbf{0} & \mathbf{D}(\bar{\mathbf{u}}) \\ \mathbf{G}(\bar{\mathbf{u}}) & \mathbf{E}(\bar{\mathbf{u}}) \end{bmatrix} \in \mathbb{R}^{n_y \times n_y}, \quad (34a)$$

$$\mathbf{H} = \begin{bmatrix} \mathbf{I} \\ \mathbf{R} \end{bmatrix} \in \mathbb{R}^{n_y \times N}, \quad \mathbf{M} \in \mathbb{R}^{n_z \times n_y} \quad (34b)$$

In eq. (33), the terms  $\bar{\mathbf{A}}$ ,  $\bar{\mathbf{B}}$ , and  $\bar{\mathbf{f}}$  are the LCM terms. The collection of matrices,

$$\boldsymbol{\Theta} = \{\mathbf{P}, \mathbf{D}(\bar{\mathbf{u}}), \mathbf{G}(\bar{\mathbf{u}}), \mathbf{\Lambda}, \mathbf{E}(\bar{\mathbf{u}}), \mathbf{Q}, \mathbf{G}(\bar{\mathbf{u}}), \mathbf{R}, \mathbf{M}\} \in \mathbb{R}^{n_\theta} \quad (35)$$

are learnable parameters to capture the memory effects. Particularly, the matrices  $\mathbf{P}, \mathbf{\Lambda}, \mathbf{Q}, \mathbf{R}$  are constants that need to be identified from data, and account for the effects of coarse-graining on the stiffness and forcing matrices. The matrices  $\mathbf{D}(\bar{\mathbf{u}}), \mathbf{E}(\bar{\mathbf{u}}), \mathbf{G}(\bar{\mathbf{u}})$  are state-dependent matrices, and account for the effects of coarse-graining on the advection matrix. Leveraging the DG-FEM formula for the advection matrix in eq. (44c) in the Appendix, and noting that the mesh displacements are functions of the ablating velocity as in eq. (3), the

state-dependent matrices for the  $i$ -th component are written as,

$$\mathbf{D}^{(i)}(\bar{\mathbf{u}}) \approx f^{(i)}(\bar{u}^{(i)})\mathbf{D}^{(i)}, \quad \mathbf{E}^{(i)}(\bar{\mathbf{u}}) \approx f^{(i)}(\bar{u}^{(i)})\mathbf{E}^{(i)}, \quad \mathbf{G}^{(i)}(\bar{\mathbf{u}}) \approx f^{(i)}(\bar{u}^{(i)})\mathbf{G}^{(i)} \quad (36)$$

where  $f^{(i)}(\bar{u}^{(i)})$  is the surface recession velocity function in eq. (12) for the  $i$ -th component, and  $\mathbf{D}^{(i)}, \mathbf{E}^{(i)}, \mathbf{G}^{(i)}$  are constant matrices to be identified from data. In eq. (33),  $\mathbf{M}$  is a fully-populated matrix that extracts the observables, i.e., the surface temperatures, from the PIROM states  $\mathbf{y}$ . The PIROM incorporates explicit information on the temperature-dependent material properties through the LCM matrices, as well as the surface recession velocity function through eq. (36). The next step is focused on identifying the unknown parameters  $\Theta$  characterizing the hidden dynamics.

### 3.3 Learning the Hidden Dynamics from Data

The learning of the PIROM is achieved through a neural-ODE like approach [Chen2018](#). For ease of presentation, consider the following compact form of the PIROM in eq. (33),

$$\mathcal{F}(\dot{\mathbf{y}}, \mathbf{y}; \boldsymbol{\xi}, \Theta) = \mathbf{0} \quad (37)$$

where  $\boldsymbol{\xi}$  defines the parametrization of the problem, i.e., operating conditions, such as the BC's, as well as the material properties. Consider a dataset of  $N_s$  high-fidelity trajectories of observables over a time interval  $[t_0, t_f]$ ,

$$\mathcal{D} = \left\{ \left( t_k, \mathbf{z}_{\text{HF}}^{(l)}(t_k), \boldsymbol{\xi}^{(l)} \right) \right\}_{l=1}^{N_s}, \quad k = 0, 1, \dots, K \quad (38)$$

The learning problem is formulated as the following differentially-constrained problem,

$$\min_{\Theta} \quad \frac{1}{N_s} \sum_{l=1}^{N_s} \frac{1}{K} \sum_{k=0}^K \left\| \mathbf{z}_{\text{HF}}^{(l)}(t_k) - \mathbf{M}\mathbf{y}^{(l)}(t_k) \right\|_2^2 \quad (39a)$$

$$\text{s.t.} \quad \mathcal{F}(\dot{\mathbf{y}}^{(l)}, \mathbf{y}^{(l)}; \boldsymbol{\xi}^{(l)}, \Theta) = \mathbf{0}, \quad t \in [t_0, t_f], \quad l = 1, 2, \dots, N_s \quad (39b)$$

$$\mathbf{y}^{(l)}(t_0) = \mathbf{y}_0(\boldsymbol{\xi}^{(l)}), \quad l = 1, 2, \dots, N_s \quad (39c)$$

## A Technical Details

This appendix presents the technical details of the PIROM framework applied to the TPS ablation problem. The first section provides the mathematical details for the definition of the DG-FEM. The second section follows the projection procedures from Ref. [x](#), and demonstrates the effects of coarse-graining on the advection matrix. The third section presents the derivation of the LCM model from an energy-conservation perspective.

### A.1 Full-Order Model

To obtain the full-order numerical solution, the governing equation is spatially discretized using variational principles of Discontinuous Galerkin (DG) to result in a high-dimensional system of ordinary differential equations (ODEs). The DG-FEM model is written in an element-wise form, which is beneficial for subsequent derivations of the lower-order models. Note that the choice of DG approach here is mainly for theoretical convenience in the subsequent coarse-graining formulation. In the numerical results, the full-order TPS ablation simulations is computed using standard FEM instead, and the equivalence between DG and standard FEM is noted upon their convergence.

#### A.1.1 Domain Discretization

Consider a conforming mesh partition of the domain, as shown in Fig. [DOMAIN](#), where each element belongs to one and only one component. Denote the collection of all  $M$  elements as  $\{E_i\}_{i=1}^M$ . To ease the description of the DG model, a graph structure is employed. The elements are treated as vertices, the set of which is denoted  $\mathcal{V} = \{m\}_{m=1}^M$ . Two neighboring elements,  $E_i$  and  $E_j$ , are connected by an edge  $(i, j)$ , and the shared boundary between them is denoted  $e_{ij}$ . The collection of all edges are denoted  $\mathcal{E}$ , and  $\mathcal{G}$  is referred to as a graph. In the graph, the edges are undirected, meaning if  $(i, j) \in \mathcal{E}$  then  $(j, i) \in \mathcal{E}$ . Furthermore, denote the neighbors of the  $i$ -th element as  $\mathcal{N}_i = \{j | (i, j) \in \mathcal{E}\}$ . Lastly, for the ease of notation, introduce two special indices:  $T$  for the boundary of an element that overlaps with the Dirichlet boundary condition, and similarly  $q$  for the Neumann boundary condition.

### 288 A.1.2 Weak Form of Discontinuous Galerkin Method

289 Choosing appropriate basis functions  $\phi_k$  and  $\phi_l$  and using the Interior Penalty Galerkin  
 290 (IPG) scheme [?], the variational bilinear form for eq. (1a) is,

$$\sum_{i=1}^M a_{\epsilon,i}(\phi_k, \phi_l) = \sum_{i=1}^M L_i(\phi_k) \quad (40)$$

291 where  $\epsilon$  is an user-specified parameter and,

$$a_{\epsilon,i}(\phi_k, \phi_l) = \int_{E^{(i)}} \left( \rho c_p \phi_k \frac{\partial \phi_l}{\partial t} + \nabla \phi_k \cdot (\mathbf{k} \nabla \phi_l) - \rho c_p \phi_k \mathbf{v} \cdot \nabla \phi_l \right) dE^{(i)} \quad (41a)$$

$$\begin{aligned} &= - \sum_{j \in \mathcal{N}_i \cup \{T_b\}} \int_{e_{ij}} \{ \mathbf{k} \nabla \phi_k \cdot \mathbf{n} \} [\phi_l] de_{ij} + \epsilon \sum_{j \in \mathcal{N}_i \cup \{T_b\}} \int_{e_{ij}} \{ \mathbf{k} \nabla \phi_l \cdot \mathbf{n} \} [\phi_k] de_{ij} \\ &+ \sigma \sum_{j \in \mathcal{N}_i \cup \{T_b\}} \int_{e_{ij}} [\phi_k] [\phi_l] de_{ij} \end{aligned} \quad (41b)$$

$$L_i(v) = \epsilon \sum_{j \in \mathcal{N}_i \cup \{T_b\}} \int_{e_{ij}} (\mathbf{k} \nabla \phi_l \cdot \mathbf{n}) T_b de_{ij} + \int_{e_{iq}} \phi_k q_b de_{iq} + \sigma \int_{e_{iT}} \phi_k T_b de_{iT} \quad (41c)$$

292 In the bi-linear form above, the notations  $[]$  and  $\{\}$  are respectively the jumps and averages  
 293 at the boundary  $e_{ij}$  share by two elements  $E_i$  and  $E_j$ ,

$$[u] = u|_{E_i} - u|_{E_j}, \quad \{u\} = \frac{1}{2} (u|_{E_i} + u|_{E_j}), \quad \text{for } x \in e_{ij} = E_i \cap E_j$$

294 Furthermore, in the bi-linear form, the terms associated with  $\sigma$  are introduced to enforce  
 295 the Dirichlet boundary conditions;  $\sigma$  is a penalty factor whose value can depend on the size  
 296 of an element. Depending on the choice of  $\epsilon$ , the bi-linear form corresponds to symmetric  
 297 IPG ( $\epsilon = -1$ ), non-symmetric IPG ( $\epsilon = 1$ ), and incomplete IPG ( $\epsilon = 0$ ). All these schemes  
 298 are consistent with the original PDE and have similar convergence rate with respect to mesh  
 299 size. In the following derivations, the case  $\epsilon = 0$  is chosen for the sake of simplicity.

### 300 A.1.3 Discontinuous Galerkin Model

301 Next, the DG-based model is written in an element-wise form. For the  $i$ -th element, use a  
 302 set of  $P$  trial functions to represent the temperature as in eq. (5). Without loss of generality,  
 303 the trial functions are assumed to be orthogonal, so that  $\int_{E^{(i)}} \phi_k^{(i)}(x) \phi_l^{(i)}(x) dx = |E^{(i)}| \delta_{kl}$ ,  
 304 where  $|E^{(i)}|$  is the area ( $n_d = 2$ ) or volume ( $n_d = 3$ ) of the  $i$ -th element, and  $\delta_{kl}$  is the  
 305 Kronecker delta.

306 Using test functions same as trial functions, the dynamics  $\mathbf{u}^{(i)}$  is obtained by evaluating



the element-wise bi-linear forms,

$$a_{\epsilon,i}(\phi_k^{(i)}, T^{(i)}) = L_i(\phi_k^{(i)}), \quad k = 1, 2, \dots, P \quad (42)$$

The above procedure yields,

$$\mathbf{A}^{(i)} \dot{\mathbf{u}}^{(i)} = (\mathbf{B}^{(i)} + \mathbf{C}^{(i)}(t)) \mathbf{u}^{(i)} + \sum_{j \in \mathcal{N}_i \cup \{T_b\}} (\mathbf{B}_{ij}^{(i)} \mathbf{u}^{(i)} + \mathbf{B}_{ij}^{(j)} \mathbf{u}^{(j)}) + \mathbf{f}^{(i)}(t) \quad (43)$$

where for  $k, l = 1, 2, \dots, P$ ,

$$[\mathbf{A}^{(i)}]_{kl} = \int_{E^{(i)}} \rho c_p \phi_k^{(i)} \phi_l^{(i)} dE^{(i)} \quad (44a)$$

$$[\mathbf{B}^{(i)}]_{kl} = - \int_{E^{(i)}} (\nabla \phi_k^{(i)}) \cdot (\mathbf{k} \nabla \phi_l^{(i)}) dE^{(i)} \quad (44b)$$

$$[\mathbf{C}^{(i)}]_{kl} = \int_{E^{(i)}} \rho c_p \phi_k^{(i)} \mathbf{v}^{(i)} \cdot \nabla \phi_l^{(i)} dE^{(i)} \quad (44c)$$

$$[\mathbf{B}_{ij}^{(i)}] = \int_{e_{ij}} \left\{ \mathbf{k} \nabla \phi_k^{(i)} \cdot \hat{n} \right\} \phi_l^{(i)} - \sigma [\phi_k^{(i)}] \phi_l^{(i)} de_{ij} \quad (44d)$$

$$[\mathbf{B}_{ij}^{(j)}] = \int_{e_{ij}} - \left\{ \mathbf{k} \nabla \phi_k^{(i)} \cdot \hat{n} \right\} \phi_l^{(j)} + \sigma [\phi_k^{(i)}] \phi_l^{(j)} de_{ij} \quad (44e)$$

$$[\mathbf{f}^{(i)}]_k = \int_{e_{iq}} \phi_k^{(i)} q_b de_{iq} + \sigma \int_{e_{iT}} \phi_k^{(i)} de_{iT} \quad (44f)$$

The matrices  $\mathbf{A}^{(i)} \in \mathbb{R}^{P \times P}$ ,  $\mathbf{B}^{(i)} \in \mathbb{R}^{P \times P}$ , and  $\mathbf{C}^{(i)} \in \mathbb{R}^{P \times P}$  are respectively the capacitance, conductivity, and advection matrices for element  $i$ . These matrices depend on  $\rho$ ,  $c_p$ ,  $\mathbf{k}$ , and  $\mathbf{v}$ , and hence can be non-linear functions of  $\mathbf{u}^{(i)}$ . Since the trial functions are orthogonal, if  $\rho c_p$  is constant within an element,  $\mathbf{A}^{(i)}$  is diagonal; otherwise,  $\mathbf{A}_i$  is symmetric and positive definite as  $\rho c_p > 0$ .

For compactness, the element-wise model in eq. (43) is also written in matrix form,

$$\mathbf{A}(\dot{\mathbf{u}}) = [\mathbf{B}(\mathbf{u}) + \mathbf{C}(\mathbf{u})] \mathbf{u} + \mathbf{f}(t) \quad (45)$$

where  $\mathbf{u} = [\mathbf{u}^{(1)}, \mathbf{u}^{(2)}, \dots, \mathbf{u}^{(M)}]^T \in \mathbb{R}^{MP}$  includes all DG variables,  $\mathbf{f} = [\mathbf{f}^{(1)}, \mathbf{f}^{(2)}, \dots, \mathbf{f}^{(M)}]^T \in \mathbb{R}^{MP}$ ,  $\mathbf{A}$  and  $\mathbf{C}$  are matrices of  $M$  diagonal blocks whose  $i$ -th blocks are  $\mathbf{A}^{(i)}$  and  $\mathbf{C}^{(i)}$ , and  $\mathbf{B}$  is a matrix of  $M \times M$  blocks whose  $(i, j)$ -th block is,

$$\mathbf{B}_{ij} = \begin{cases} \mathbf{B}^{(i)} + \sum_{j \in \mathcal{N}_i \cup \{T_b\}} \mathbf{B}_{ij}^{(i)}, & i = j \\ \mathbf{B}_{ij}^{(j)}, & i \neq j \end{cases} \quad (46)$$

319 The dependency of  $\mathbf{A}$ ,  $\mathbf{B}$ , and  $\mathbf{C}$  on  $\mathbf{u}$  is explicitly noted in eq. (45), which is the source of  
 320 non-linearity in the current TPS problem. Moreover, the mesh velocity  $\mathbf{v}$  varies with space  
 321 and time, and thus the advection matrix  $\mathbf{C}$  varies with time as a function of  $q_b$ .

## 322 A.2 Coarse-Graining of Dynamics

323 The LCM is obtained by coarse-graining the full-order DG-FEM. This coarse-graining proce-  
 324 dure produces resolved  $\mathbf{r}^{(1)}(\mathbf{u}, t)$  and residual  $\mathbf{r}^{(2)}(\mathbf{u}, t)$  dynamics as in eq. (20). This section  
 325 presents the detail derivations and magnitude analysis for the resolved and residual dynam-  
 326 ics.

### 327 A.2.1 Resolved Dynamics

328 Using eq. (17), the resolved dynamics is computed as follows,

$$\mathbf{r}^{(1)}(\mathbf{u}, t) = \mathcal{P} [\Phi^+ \mathbf{A}(\mathbf{u})^{-1} (\mathbf{B}(\mathbf{u})\mathbf{u} + \mathbf{C}(\mathbf{u})\mathbf{u} + \mathbf{f}(t))] \quad (47a)$$

$$\begin{aligned} &= \Phi^+ \mathbf{A}(\mathbf{P}\mathbf{u})^{-1} \mathbf{P}\mathbf{B}(\mathbf{P}\mathbf{u}) \mathbf{P}\mathbf{u} + \Phi^+ \mathbf{A}(\mathbf{P}\mathbf{u})^{-1} \mathbf{P}\mathbf{C}(\mathbf{P}\mathbf{u}) \mathbf{P}\mathbf{u} \\ &\quad + \Phi^+ \mathbf{A}(\mathbf{P}\mathbf{u})^{-1} \mathbf{P}\mathbf{f}(t, \mathbf{P}\mathbf{u}) \end{aligned} \quad (47b)$$

$$\begin{aligned} &= \underbrace{\Phi^+ \mathbf{A}(\Phi\bar{\mathbf{u}})^{-1} \Phi}_{\#1} \underbrace{\Phi^+ \mathbf{B}(\Phi\bar{\mathbf{u}}) \Phi\bar{\mathbf{u}}}_{\#2} + \Phi^+ \mathbf{A}(\Phi\bar{\mathbf{u}})^{-1} \Phi \underbrace{\Phi^+ \mathbf{C}(\Phi\bar{\mathbf{u}}) \Phi\bar{\mathbf{u}}}_{\#3} \\ &\quad + \Phi^+ \mathbf{A}(\Phi\bar{\mathbf{u}})^{-1} \Phi \underbrace{\Phi^+ \mathbf{f}(t, \Phi\bar{\mathbf{u}})}_{\#4} \end{aligned} \quad (47c)$$

329 Detailed derivations for the #1, #2, and #4 terms can be found in Ref. [x](#). The effects of  
 330 coarse-graining on the advection term #3 are analyzed next.

331 **Term #3** The  $\mathbf{C}(\mathbf{u}) \in \mathbb{R}^{MP \times MP}$  matrix contains  $M$  diagonal of size  $P \times P$ , since the  
 332 basis functions are defined locally on each element. Therefore,  $[\mathbf{C}(\mathbf{u})]_{ij} = \mathbf{0}$  for all  $i \neq j$  with  
 333  $i, j = 1, 2, \dots, M$ . It follows that for  $k, l = 1, 2, \dots, N$ ,

$$[\Phi^+ \mathbf{C}(t, \Phi\bar{\mathbf{u}}) \Phi]_{kl} = \sum_{i=1}^M \sum_{j=1}^M \varphi_i^{k+} [\mathbf{C}(t, \Phi\bar{\mathbf{u}})]_{ij} \varphi_j^l \quad (48a)$$

$$= \sum_{i=1}^M \varphi_i^{k+} [\mathbf{C}(t, \Phi\bar{\mathbf{u}})]_{ii} \varphi_i^l \quad (48b)$$

$$= \sum_{i \in \mathcal{V}_k} \varphi_i^{k+} [\mathbf{C}(t, \Phi\bar{\mathbf{u}})]_{ii} \varphi_i^l \quad (48c)$$

334 where in the second row, the fact that  $[\mathbf{C}(\mathbf{u})]_{ij} = 0$  for all  $i \neq j$  is used, and in the last row,  
 335 the fact that  $\varphi_i^{k+} = 0$  for all  $i \notin \mathcal{V}_k$  is used. Now, considering that  $[\mathbf{C}(\mathbf{u})]_{ii}$  has a (1,1)-th  
 336 zero element, i.e.,  $[C_{11}(t, \Phi \bar{\mathbf{u}})]_{ii} = 0$ , and that if  $k \neq l$  then  $i \notin \mathcal{V}_l$  and thus  $\varphi_i^l = \mathbf{0}$ , it follows  
 337 that for some index  $i \in \mathcal{V}_k$ ,

$$\varphi_i^{k+} [\mathbf{C}(t, \Phi \bar{\mathbf{u}})]_{ii} \varphi_i^l = \varphi_i^{k+} [\mathbf{C}(t, \Phi \bar{\mathbf{u}})]_{ii} \varphi_i^k = \frac{|E_i|}{|\Omega_k|} [C_{11}(t, \Phi \bar{\mathbf{u}})]_{ii} = 0 \quad (49)$$

338 The matrix  $[\Phi^+ \mathbf{C}(t, \Phi \bar{\mathbf{u}}) \Phi]_{kl} = 0$  for all  $k, l = 1, 2, \dots, N$ , and thus,

$$\bar{\mathbf{C}}(t, \bar{\mathbf{u}}) = \Phi^+ \mathbf{C}(t, \Phi \bar{\mathbf{u}}) \Phi = \mathbf{0} \quad (50)$$

339 as indicated by the LCM in eq. (8).

### 340 A.2.2 Magnitude Analysis for Residual Dynamics

341 Next, the magnitude of the residual dynamics  $\mathbf{r}^{(2)}(\mathbf{u}, t)$  is analyzed to pinpoint the missing  
 342 physics in the LCM. By definition,

$$\mathbf{r}^{(2)}(\mathbf{u}, t) = \dot{\bar{\mathbf{u}}} - \mathbf{r}^{(1)}(\bar{\mathbf{u}}, t) \quad (51a)$$

$$= \Phi^+ \mathbf{r}(\mathbf{u}, t) - \mathbf{r}^{(1)}(\mathbf{u}, t) \quad (51b)$$

$$\begin{aligned} &= \underbrace{\Phi^+ \mathbf{A}(\mathbf{u})^{-1} \mathbf{B}(\mathbf{u}) \mathbf{u} - \bar{\mathbf{A}}(\bar{\mathbf{u}})^{-1} \bar{\mathbf{B}}(\bar{\mathbf{u}}) \bar{\mathbf{u}}}_{\#1} + \underbrace{\Phi^+ \mathbf{A}(\mathbf{u})^{-1} \mathbf{C}(\mathbf{u}) \mathbf{u} - \bar{\mathbf{A}}(\bar{\mathbf{u}})^{-1} \bar{\mathbf{C}}(t, \bar{\mathbf{u}}) \bar{\mathbf{u}}}_{\#2} \\ &\quad + \underbrace{\Phi^+ \mathbf{A}(\mathbf{u})^{-1} \mathbf{f}(t) - \bar{\mathbf{A}}(\bar{\mathbf{u}})^{-1} \bar{\mathbf{f}}(t)}_{\#3} \end{aligned} \quad (51c)$$

343 The magnitude analysis for terms #1 and #3 can be found in Ref. [x](#). The analysis for term  
 344 #2 is presented next. Let  $\mathbf{D}(\bar{\mathbf{u}}) = \mathbf{A}(\Phi \bar{\mathbf{u}})^{-1} \mathbf{P} \mathbf{C}(t, \Phi \bar{\mathbf{u}})$ , then,

$$\Phi^+ \mathbf{A}(\mathbf{u})^{-1} \mathbf{C}(\mathbf{u}) \mathbf{u} - \bar{\mathbf{A}}(\bar{\mathbf{u}})^{-1} \bar{\mathbf{C}}(t, \bar{\mathbf{u}}) \bar{\mathbf{u}} \quad (52a)$$

$$= \Phi^+ \mathbf{A}(\mathbf{u})^{-1} \mathbf{C}(\mathbf{u}) \mathbf{u} - \Phi^+ \mathbf{A}(\Phi \bar{\mathbf{u}})^{-1} \mathbf{P} \mathbf{C}(t, \Phi \bar{\mathbf{u}}) \Phi \Phi^+ \mathbf{u} \quad (52b)$$

$$= \Phi^+ \mathbf{A}^{-1}(\mathbf{u}) \mathbf{C}(\mathbf{u}) \mathbf{u} - \Phi^+ \mathbf{D}(\bar{\mathbf{u}}) \Phi \Phi^+ \mathbf{u} \quad (52c)$$

$$(52d)$$

where  $\mathbf{P} = \Phi\Phi^+$ . Thus,

$$\|\Phi^+ \mathbf{A}(\mathbf{u})^{-1} \mathbf{C}(\mathbf{u}) \mathbf{u} - \bar{\mathbf{A}}^{-1}(\bar{\mathbf{u}}) \bar{\mathbf{C}}(t, \bar{\mathbf{u}}) \bar{\mathbf{u}}\| \quad (53a)$$

$$\leq \|\Phi^+ \mathbf{A}^{-1}(\mathbf{u}) \mathbf{C}(\mathbf{u}) \mathbf{u} - \Phi^+ \mathbf{D}(\bar{\mathbf{u}}) \mathbf{u}\| + \|\Phi^+ \mathbf{D}(\bar{\mathbf{u}}) \mathbf{u} - \Phi^+ \mathbf{D}(\bar{\mathbf{u}}) \Phi \Phi^+ \mathbf{u}\| \quad (53b)$$

$$\leq \|\Phi^+\| \underbrace{\|\mathbf{A}^{-1}(\mathbf{u}) \mathbf{C}(\mathbf{u}) \mathbf{u} - \mathbf{D}(\bar{\mathbf{u}}) \mathbf{u}\|}_{\#1} + \|\Phi^+ \mathbf{D}(\bar{\mathbf{u}})\| \underbrace{\|\mathbf{u} - \Phi \Phi^+ \mathbf{u}\|}_{\#2} \quad (53c)$$

where term #2 is due to the approximation of non-uniform temperature as constants, and term #1 is the error in the advection dynamics due to coarse-graining.

### A.3 Lumped Capacitance Model

The following assumptions are employed: (1) the temperature in component ( $i$ ) is described by a scalar time-varying average temperature  $\bar{u}^{(i)}$ , (2) between neighboring components ( $i$ ) and ( $j$ ) the heat flux is approximated as,

$$q_{ij} = \frac{\bar{u}^{(j)} - \bar{u}^{(i)}}{R_{ij}} \quad (54)$$

where  $R_{ij}$  is the thermal resistance. Empirically, for a component of isotropic heat conductivity  $k$ , length  $\ell$ , and cross-section area  $A$ , the thermal resistance is  $R = \ell/kA$ . Between components  $i$  and  $j$ , define  $R_{ij} = R_i + R_j$ . In addition, the heat flux due to Dirichlet boundary condition is computed as  $q_{iT} = (T_b - \bar{u}^{(i)})/R_i$ .

At component  $i$ , the dynamics of LCM are given by,

$$\int_{E^{(i)}} \rho c_p \dot{\bar{u}}^{(i)} dE^{(i)} = \left( \sum_{j \in \mathcal{N}_i} \int_{e_{ij}} \frac{\bar{u}^{(j)} - \bar{u}^{(i)}}{R_{ij}} de_{ij} \right) + \int_{e_{iq}} q_b de_{iq} + \int_{e_{iT}} \frac{T_b - \bar{u}^{(i)}}{R_i} de_{iT} \quad (55a)$$

$$\bar{A}^{(i)} \dot{\bar{u}}^{(i)} = \left( \sum_{j \in \mathcal{N}_i} \frac{|e_{ij}|}{R_{ij}} (\bar{u}^{(j)} - \bar{u}^{(i)}) \right) + |e_{iq}| \bar{q}^{(i)} + \frac{|e_{iT}|}{R_i} (\bar{T}^{(i)} - \bar{u}^{(i)}) \quad (55b)$$

$$= \sum_{j \in \mathcal{N}_i} \left( -\frac{|e_{ij}|}{R_{ij}} \bar{u}^{(i)} + \frac{|e_{ij}|}{R_{ij}} \bar{u}^{(j)} \right) + \left( -\frac{|e_{iT}|}{R_i} \bar{u}^{(i)} \right) + \left( |e_{iq}| \bar{q}^{(i)} + \frac{|e_{iT}|}{R_i} \bar{T}^{(i)} \right) \quad (55c)$$

$$= \sum_{j \in \mathcal{N}_i \cup \{T_b\}} \left( \bar{B}_{ij}^{(i)} \bar{u}^{(i)} + \bar{B}_{ij}^{(j)} \bar{u}^{(j)} \right) + \bar{f}^{(i)} \quad (55d)$$

where in eq. (55b)  $|e|$  denotes the length ( $d = 2$ ) or area ( $d = 3$ ) of a component boundary  $e$ . The  $\bar{A}^{(i)}$ ,  $\bar{B}_{ij}^{(i)}$ , and  $\bar{B}_{ij}^{(j)}$  quantities are provided in eq. (11).

The lumped-mass representation for the four-component TPS is shown in Fig. 2. Let  $v_i$

360 represent the area of the  $i$ -th element,  $\overline{\rho c_{p,i}}$ , the heat capacity evaluated using the average  
 361 temperature  $\bar{u}^{(i)}$ , and  $1/R_{ij} = 1/R_i(\bar{u}^{(i)}) + 1/R_j(\bar{u}^{(j)})$  the equivalent thermal resistance  
 362 between elements  $i$  and  $j$ . Leveraging the formulas from eqs. (10) and (11), the LCM  
 363 matrices are given by,

$$\bar{\mathbf{A}} = \begin{bmatrix} \overline{\rho c_{p,1}} v_1 & 0 & 0 & 0 \\ 0 & \overline{\rho c_{p,2}} v_2 & 0 & 0 \\ 0 & 0 & \overline{\rho c_{p,3}} v_3 & 0 \\ 0 & 0 & 0 & \overline{\rho c_{p,4}} v_4 \end{bmatrix}, \quad (56a)$$

$$\bar{\mathbf{B}} = \begin{bmatrix} \frac{1}{R_{12}} + \frac{1}{R_{14}} & -\frac{1}{R_{12}} & 0 & -\frac{1}{R_{14}} \\ -\frac{1}{R_{12}} & \frac{1}{R_{12}} + \frac{1}{R_{24}} + \frac{1}{R_{23}} & -\frac{1}{R_{23}} & -\frac{1}{R_{24}} \\ 0 & -\frac{1}{R_{32}} & \frac{1}{R_{32}} + \frac{1}{R_{34}} & -\frac{1}{R_{34}} \\ -\frac{1}{R_{14}} & -\frac{1}{R_{24}} & -\frac{1}{R_{34}} & \frac{1}{R_{14}} + \frac{1}{R_{24}} + \frac{1}{R_{34}} \end{bmatrix}, \quad \bar{\mathbf{f}} = \begin{bmatrix} \bar{q}^{(1)} \\ \bar{q}^{(2)} \\ \bar{q}^{(3)} \\ 0 \end{bmatrix} \quad (56b)$$